1   **Do land surface models capture the seasonality of carbon fluxes in the Amazon basin?**

2   **A data-model intercomparison**

3

4   **Running head:** Seasonal C-flux simulations at Amazon forests

5   Natalia Restrepo-Coupe[1,2], Naomi Levine[3,4], Bradley O'Donnell Christoffersen[2,5,8], Loren Albert[2],

6   Jin Wu[2], Marcos H. Costa[7], David Galbraith[6], Hewlley Imbuzeiro[7], Giordane Martins[12], Alessandro

7   C. da Araujo[9,10], Yadvinder S. Malhi[11], Xubin Zeng[8], Paul Moorcroft[4], and Scott R. Saleska[2]

8

9   (1)   Plant Functional Biology and Climate Change Cluster, University of Technology Sydney, Sydney, NSW,

10   Australia.

11   (2)   Department of Ecology and Evolutionary Biology, University of Arizona, Tucson, AZ, USA.

12   (3)   College of Letters, Arts, and Science, University of Southern California, Los Angeles, CA, USA.

13   (4)   Department of Organismic and Evolutionary Biology, Harvard University, Cambridge, MA, USA.

14   (5)   Earth and Environmental Sciences Division, Los Alamos National Laboratory, Los Alamos, NM, USA.

15   (6)   School of Geography, University of Leeds, Leeds, UK.

16   (7)   Department of Agricultural Engineering, Federal University of Vicosa, Vicosa, MG, Brazil.

17   (8)   Department of Atmospheric Sciences, University of Arizona, Tucson, AZ, USA.

18   (9)   Instituto Nacional de Pesquisas da Amazônia (INPA), Manaus, Amazonas, Brazil.

19   (10)   Embrapa Amazônia Oriental, Belem, Para, Brazil.

20   (11)   Environmental Change Institute, School of Geography and the Environment, University of Oxford, Oxford,

21   UK.

22   (12)   Instituto Nacional de Pesquisas da Amazônia (INPA), Manaus, Amazonas, Brazil.

23

24   **Correspondence:** Natalia Restrepo-Coupe, tel. +1 647 328 1474, email <u>nataliacoupe@gmail.com</u>

25   **Key words:** Carbon dynamics, seasonality, Amazon, tropical forests phenology, land surface model

26   **Type of Paper:** Primary Research Article

28   **Abstract**

29   To predict forest response to long-term climate change with confidence requires that land surface

30   models (LSMs) first be successfully tested against ecosystem response to short-term variations in

31   environmental drivers, including regular seasonal patterns. Here, we use an integrated dataset from

32   four forests in the Brasil flux network, spanning a range of dry season intensities and lengths, to test

33   how well four state-of-the-art models (IBIS, ED2, JULES, and CLM3.5) simulate the seasonality of

34   carbon exchanges in Amazonian tropical forests. We found that most LSMs poorly represent the

35   annual cycle of gross primary productivity (GPP), photosynthetic capacity (Pc, a proxy for

36   phenology), and other fluxes and pools. Specifically, our analysis shows that models simulated

37   consistent dry season declines in GPP in the equatorial Amazon (Manaus K34, Santarem K67, and

38   Caxiuana CAX); however, observed GPP increased. Model predicted GPP reductions are driven

39   by "soil water stress" and in some cases a constant or decreasing photosynthetic infrastructure (e.g.

40   Pc, and leaf area index (LAI)). Nevertheless, at this rainforests, observed dry-season increasing

41   incoming radiation, leaf-flush and abscission, and/or Pc result in higher uptake. Similarly, we

42   report divergences between model-observed seasonal net ecosystem exchange (NEE) and

43   respiration (Re) at equatorial locations. By contrast, at the southern Amazon forest (Jarú RJA)

44   observed declines in GPP and Re as the dry season progresses are well represented by most LSMs.

45   While the (1) water-limitation mechanism is described in models and the primary driver of seasonal

46   photosynthesis in southern Amazonia, we identify other biophysical processes: (2) light harvesting

47   adaptations (e.g. LAI and/or leaf-level assimilation rate increases related to leaf demography); and

48   (3) allocation schemes (e.g. lags between leaf and wood production) that are poor or absent in

49   current model formulations. All three mechanisms dominate equatorial Amazon carbon flux

50   dynamics and are critical for correctly simulating flux seasonality at tropical forests.

51

1.   Introduction

Land surface models (LSMs) are the most widely used and appropriate tool for predicting large-scale responses of vegetation to future climate scenarios. However, to forecast the future of Amazonia under climate change remains a challenge. The previous generation of LSMs produced projections of Amazonia's future that diverged widely, with outcomes ranging from large-scale forest die-back to forest resilience (Betts *et al.*, 2004, 2004; Friedlingstein *et al.*, 2006; Baker *et al.*, 2008). More recent LSMs simulations showed the large-scale die-off scenario to be unlikely (Cox *et al.*, 2013), given (1) an improved model understanding of forest response to the negative effects of temperature -previously overestimated and now constrained (Cox *et al.*, 2013); and (2) current models being forced with updated climate projections (temperature and precipitation) bounded by observations that no longer demonstrate drastic climate changes in response to rising CO_2 in the tropics (Cox *et al.*, 2013; Huntingford *et al.*, 2013). Yet tropical forest response to climate change remains uncertain as models produce varying outcomes (Shao *et al.*, 2013) even without die-off. Some cutting-edge LSMs projected forest degradation due to future deforestation and increasing temperature, with catastrophic consequences for the global climate based on climate-carbon cycle feedbacks (Wang *et al.*, 2013, 2014; Friend *et al.*, 2014), while other LSMs foresaw strong carbon sinks in these forests due to CO_2 fertilization of photosynthesis (Rammig *et al.*, 2010; Ahlström *et al.*, 2012; Huntingford *et al.*, 2013; Friend *et al.*, 2014). Although the effects of temperature, water limitation and CO_2 fertilization mechanisms remain uncertain, all LSMs continue to agree that Amazonian forests play an important role in regulating the global carbon and water cycle (Eltahir & Bras, 1994; Werth & Avissar, 2002; Wang *et al.*, 2013, 2014; Ahlström *et al.*, 2015).

Key to reducing uncertainty in LSMs is their systematic evaluation against observational datasets.

75   This exercise enables the identification of model deficiencies through comparison with observed

76   patterns in ecosystem processes, as well as the mechanisms underpinning such processes (Baker *et*

77   *al.,* 2008; Christoffersen *et al.,* 2014). Recent model-data evaluations in tropical forests have

78   focused on the cascade of ecosystem responses to long term droughts (Powell *et al.,* 2013) and the

79   definition of spatial patterns in productivity and biomass (Delbart *et al.,* 2010; Castanho *et al.,*

80   2013). However, one important context for model assessment in tropical forests is in the

81   seasonality of ecosystem water and carbon exchange, as observational datasets reveal axes of

82   variation in productivity, biomass and/or forest function across space (da Rocha *et al.,* 2009;

83   Restrepo-Coupe *et al.,* 2013) and/or through time (Saleska *et al.,* 2003; von Randow *et al.,* 2004;

84   Hutyra *et al.,* 2007; Brando *et al.,* 2010). The most consistent temporal variation in tropical forests

85   is the seasonality of water, energy, and carbon exchange, since all tropical ecosystems are seasonal

86   in terms of insolation and a majority experience recurrent changes in precipitation, temperature

87   and/or day length. Evaluation with respect to seasonality has typically focused on

88   evapotranspiration (*ET*) (Shuttleworth, 1988; Werth & Avissar, 2002; Christoffersen *et al.,* 2014)

89   and on net carbon exchange (*NEE*) (Baker *et al.,* 2008; von Randow *et al.,* 2013; Melton *et al.,*

90   2015). Where models compensated misrepresentations of gross primary productivity (*GPP*) in the

91   *NEE* balance, by improving or adjusting the efflux term represented by heterotrophic (Melton *et al.,*

92   2015) or ecosystem respiration (Baker *et al.,* 2008) to available moisture among other strategies.

93   Only recently have the seasonal dynamics of *GPP* drawn the attention of different groups (De

94   Weirdt *et al.,* 2012; Kim *et al.,* 2012) and where Kim et al. (2012) demonstrated that a consequence

95   of its incorrect derivation was to overestimate the vulnerability of tropical forests to climate

96   extremes. Therefore, identifying discrepancies in observed *versus* modeled seasonality in carbon

97   flux even when seasonal amplitudes are not large -as can be the case for evergreen tropical forests

98   (see Albert et al. (in preparation) for cryptic phenology), can lead to important model developments

99   with significant consequences -to obtain better projections of the fate of tropical ecosystems under

100   present and future climate scenarios.

101

102   Analysis of eddy covariance datasets have shown that in non-water limited forests of Amazonia, the

103   observed seasonality of *GPP* was not exclusively controlled by seasonal variations in light quantity

104   (as has been demonstrated for *ET*) or water availability. Instead *GPP* was driven by a combination

105   of incoming radiation and phenological rhythms influencing leaf quantity (measured as leaf area

106   index; *LAI*) and quality (leaf-level photosynthetic capacity as a function of time since leaf flush)

107   (Wu *et al.*, submitted; Restrepo-Coupe *et al.*, 2013).   The lack of a direct correlation between *GPP*

108   and climate suggests that ecosystem models that are missing sufficient detail of canopy leaf

109   phenology will likely not capture seasonal productivity patterns. Accordingly, recent studies

110   showed model simulations (ED2 and ORCHIDEE) to be deficient in terms of predicted seasonality

111   in *GPP* and litterfall, if missing leaf-demography and turnover as in Kim et al. (2012) and in De

112   Weirdt et al. (2012), respectively. Between the two studies, only two sites (eastern (K67) and

113   northeastern (CAX)) were represented, both of which experience very similar precipitation and light

114   regimes. This further highlights the need for expanded evaluation of modeled seasonality of *GPP*

115   across a range of sites spanning a broader range of climates and phenologies.

116

117   If the improved representation of the dynamics of leaves and other carbon pools, translates into

118   more accurate simulations of seasonal *GPP, NEE* and/or the long-term carbon budget (De Weirdt

119   *et al.*, 2012; Kim *et al.*, 2012; Melton *et al.*, 2015), then comparisons between observations and

120   model derived seasonality of carbon allocation, could provide insight into the mechanistic response

121   of vegetation to climate and strategies to incorporate them into LSMs. For example, critically

122   evaluating the seasonality of net primary production of leaves (NPP_{leaf}) and wood (NPP_{wood}) in

123 tandem with *GPP,* will inform deficiencies in model allocation schemes and carbon pool residence

124 times. Model net primary production (*NPP)* typically arises from the allocation of photosynthate to

125 main organs, either as a constant fraction of *GPP* (Kucharik *et al.,* 2006), or according to fixed

126 allometric rules (Sitch *et al.,* 2003). However, such a view of supply-limited growth has come into

127 question recently (Würth *et al.,* 2005; Fatichi *et al.,* 2014). Thus as water, temperature, and

128 nutrients can all impact cell expansion, there may be a temporary imbalance between carbon used

129 for tissue growth and maintenance respiration *versus* carbon supplied by assimilation

130 (photosynthesis) (Fatichi *et al.,* 2014). Patterns in seasonality of *GPP, NPP_{leaf}* and *NPP_{wood},*

131 therefore, potentially reveal the degree of coupling (or lack thereof) of these two carbon sinks

132 (*NPP_{wood}* and *NPP_{leaf}*) with photosynthetic activity (*GPP*). Indeed, Doughty et al. (2014) used

133 bottom-up estimates of the ecosystem carbon-budget at a forest in southwest Amazonia and showed

134 that components of *NPP* varied independently of photosynthetic supply, which they interpreted in

135 terms of theories of optimal allocation patterns. While an alternative interpretation of such patterns

136 could simply refer to biophysical limitations on growth, which vary seasonally (Fatichi *et al.,* 2014),

137 both studies suggest that modeling allocation as a function of *GPP* will likely fail to capture

138 observed seasonality. Ground-based bottom-up estimates of primary productivity at a temporal

139 resolution greater than a year (i.e., seasonal) are difficult if not impossible, principally because there

140 is no accepted method for estimating whole-tree non-structural carbon (*NSC*) and its variation with

141 seasons (Würth *et al.,* 2005; Richardson *et al.,* 2015). We proposed coupling co-located top-down

142 eddy flux estimates of *GPP* with bottom-up *NPP* estimates (*NPP_{wood}, NPP_{leaf}* and *$NPP_{litter-fall}$*) to

143 circumvent this problem and to obtain a better informed view of the mechanisms (e.g. allocation

144 schemes) models may incorporate or test against, to improve seasonal simulations of carbon fluxes

145 and pools.

146

147   The focus of this study was to evaluate, for the first time, modeled seasonal cycles of different

148   carbon pools and fluxes, including leaf area index (*LAI*), *GPP*, leaf fall, leaf flush, and wood

149   production, with high resolution eddy flux estimates of *GPP* and ground-based surveys. We

150   centered our study on a comparison between forests located in the equatorial Amazon (radiation-

151   and phenology-driven) to a southern forest (driven by water availability) and explored the different

152   model strategies to incorporate and simulate physical and ecological drivers. Here, we assessed

153   four state-of-the art LSMs in active development for use in coupled climate-carbon cycle

154   simulations in terms of whether they could simultaneously determine patterns of growth and

155   photosynthesis, thereby getting the 'right answer for the right reason'. We conclude by proposing

156   several approaches for improving model formulations and highlight the need for model-informed

157   field campaigns and future experimental designs.

158

159   **2.   Methods**

160   **2.1.Site descriptions**

161   We analyzed data from the Brazil flux network for four tropical forests represented by the southern

162   site of Reserva Jarú (RJA), and three central Amazonia forests (~3ºS) from west to east: the Reserva

163   Cuieiras near Manaus (K34), the Tapajós National forest, near Santarém (K67) , and the Caxiuanã

164   National forest near Belém (CAX) (Fig. 1). For detailed site information see previous works by

165   Restrepo-Coupe et al. (2013), and de Goncalves et al. (2009; 2013) and individual site publications

166   (Araújo *et al.*, 2002; Carswell *et al.*, 2002; Malhi *et al.*, 2002; Saleska *et al.*, 2003; Kruijt *et al.*,

167   2004; von Randow *et al.*, 2004; Hutyra *et al.*, 2007; da Costa *et al.*, 2010).

168
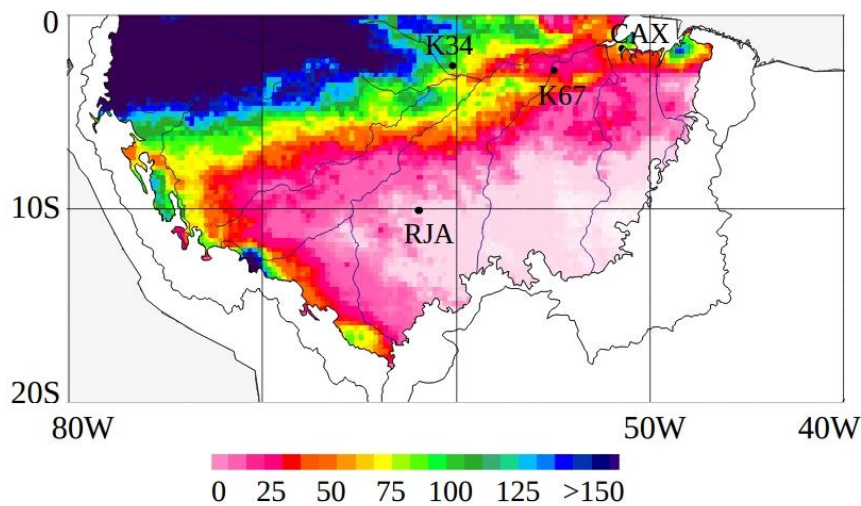
Figure 1. Locations eddy covariance tower study sites at the Amazon Basin *sensu-stricto (Eva &*

Huber (eds), 2005). Monthly minimum precipitation from the Tropical Rainfall Measuring Mission

(TRMM) (NASA, 2014) based on an annual composite for the years 1998 to 2014.

All study sites had mean annual precipitation (*MAP*) above 2000 mm year^{-1} (Supplement Fig. 1),

based on the satellite-derived precipitation from the Tropical Rainfall Measuring Mission (TRMM)

(Huffman *et al.*, 2007; NASA, 2014) 1998-2013 (Table 1). CAX and K34 have *MAP* over 2500

mm year^{-1} (2572 and 2674mm year^{-1}, respectively). By contrast, at the southern forest of RJA and

the equatorial forest of K67 *MAP* was ~2030 mm year^{-1}. Moreover, RJA has a 5-month dry season

length (*DSL*) analogous to two of the central Amazon sites of CAX and K67 (4-month); however,

longer than K34 site (2-months). Where the dry season was defined as those periods where

precipitation is less than ~100 mm month^{-1}, this threshold corresponded to 80% of the average

monthly *ET* observed at tropical forests (Sombroek, 2001; da Rocha *et al.*, 2004; Restrepo-Coupe *et*

al., 2013). RJA and K67 showed similar mean dry-season precipitation (47 mm month^{-1} at RJA and

54 mm month^{-1} at K67). However, the annual minimum averaged across the years 1998-2014

(*MiAP*) at RJA was 14 mm month^{-1} compared to a more benign dry season minimum of 37 mm

month^{-1} at K67 (Fig. 1 and Table 1). Despite being located at a latitude further from the equator

8

186 (10°S) incoming photosynthetic active radiation (*PAR*) at the southern forest of Jarú, was less

187 seasonal (low amplitude) if compared to the central Amazon forests (latitude ~3°S) (Fig. 2). At

188 RJA, peak top of the atmosphere radiation (*TOA*) was synchronous to the wet season – where we

189 expected higher reflectance by clouds decreasing the surface available *PAR* (Fig. 2). All equatorial

190 sites sat on highly weathered deep clay soils (>= 10 m), whereas RJA sat on a lower water storage

191 capacity loamy sandy soil and a more shallow and variable profile, with depth to bedrock as

192 shallow as 2-3 m (Hodnett *et al.*, 1996; Christoffersen *et al.*, 2014).

193

Site	Latitude	Longitude	Mean annual precipitation *MAP* [mm/month]	Dry season precipitation *DSP* [mm/month]	Dry season length *DSL* [months]	Minimum annual precipitation *MiAP* [mm/month]
K34	-2.61	-60.21	2674	105	2**	103
CAX	-1.72	-51.53	2572	78	4	60
K67	-2.86	-54.96	2035	54	4	37
RJA	-10.08	-61.93	2031	47	5	14

** Defined as Rain<110 mm/month, 100 mm/month at other sites
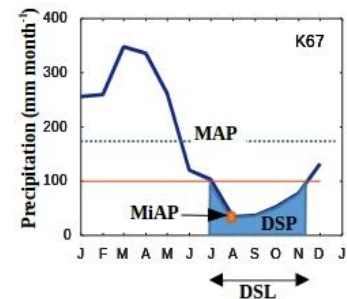
194

195 Table 1. Precipitation at Amazon basin study sites. Based on the Tropical Rainfall Measuring

196 Mission (TRMM) (NASA, 2014) for the years 1998 to 2014.

197

198   **2.2.Eddy covariance methods**

199 At the above-mentioned forests, climate, carbon, energy, water and momentum fluxes were

200 measured by the eddy covariance (EC) method. Starting with half-hourly CO_2-flux data provided

201 from each site's operator, we calculated net ecosystem exchange (*NEE* in µmol CO_2 m^{-2} s^{-1}), with

202 fluxes to the atmosphere defined as positive. *NEE* was then filtered it for low turbulence periods

203 ($u*_{thresh}$). For a detailed description of instrumentation, applied corrections, quality control

204 procedures, and methods for data processing refer to Restrepo-Coupe et al. (2013). Gross

205 ecosystem exchange (*GEE*) was derived from tower measurements of daytime *NEE* by subtracting

206   estimates of ecosystem respiration (R_{eco}), which in turn we derived from the nighttime *NEE*. We

207   assumed daytime R_{eco} was the same as nighttime R_{eco}. *GEE* is a negative value (*GEE* = *NEE* - R_{eco})

208   as generally *NEE* is negative in the daytime, and R_{eco} is positive (meteorological convention). We

209   expressed ecosystem-scale photosynthesis, or gross ecosystem productivity (*GEP*), as negative *GEE*

210   and assumed negligible re-assimilation of metabolic respiration CO_2 within the leaf and

211   insignificant CO_2 recirculation below the EC system (Stoy *et al.*, 2006). For comparison with

212   model output, we assumed negligible seasonal changes in photorespiration and used *GEP*

213   interchangeably with gross primary productivity (*GPP*).

214

215   We defined ecosystem photosynthetic capacity (*Pc*, $gC\,m^{-2}\,d^{-1}$) as the 16-day average *GPP* at a

216   fixed photosynthetically active radiation (*PAR*) range (site specific daytime mean *PAR*, PAR_{avg} ±

217   100 $\mu mol\,m^{-2}\,s^{-1}$) (Supplement Table 1); thus, to remove the effect of day-to-day changes in

218   available light (e.g. cloudy *versus* clear days), photoperiod, and any other effect of non-optimum

219   *PAR* levels. Similarly we used vapor pressure deficit (*VPD*), air temperature (T_a) to remove *GPP*

220   measures obtained during non-optimum conditions by restricting *Pc* calculations to mean daytime

221   *VPD* (VPD_{avg}) and T_a ($T_{a\,avg}$) ± one standard deviation from their respective time series. *Pc*

222   represents the vegetation built capacity to do photosynthesis (*Pc* as biophysical driver of *GPP*).

223   Where at the four study sites, it has been shown that the seasonal pattern of *Pc* was independent of

224   and other climatic variables (Restrepo-Coupe *et al.*, 2013).

225

226   We looked at evapotranspiration (*ET*, $mm\,d^{-1}$) calculated as the latent heat flux (*LE*, $W\,m^{-2}$)

227   measured at the tower multiplied by the latent heat of vaporization (λ, $kJ\,kg^{-1}$). We developed a

228   Type II linear model between surface incident short wave radiation (SW_{down}, $W\,m^{-2}$) and the

229   dependent variable, *ET*.

230
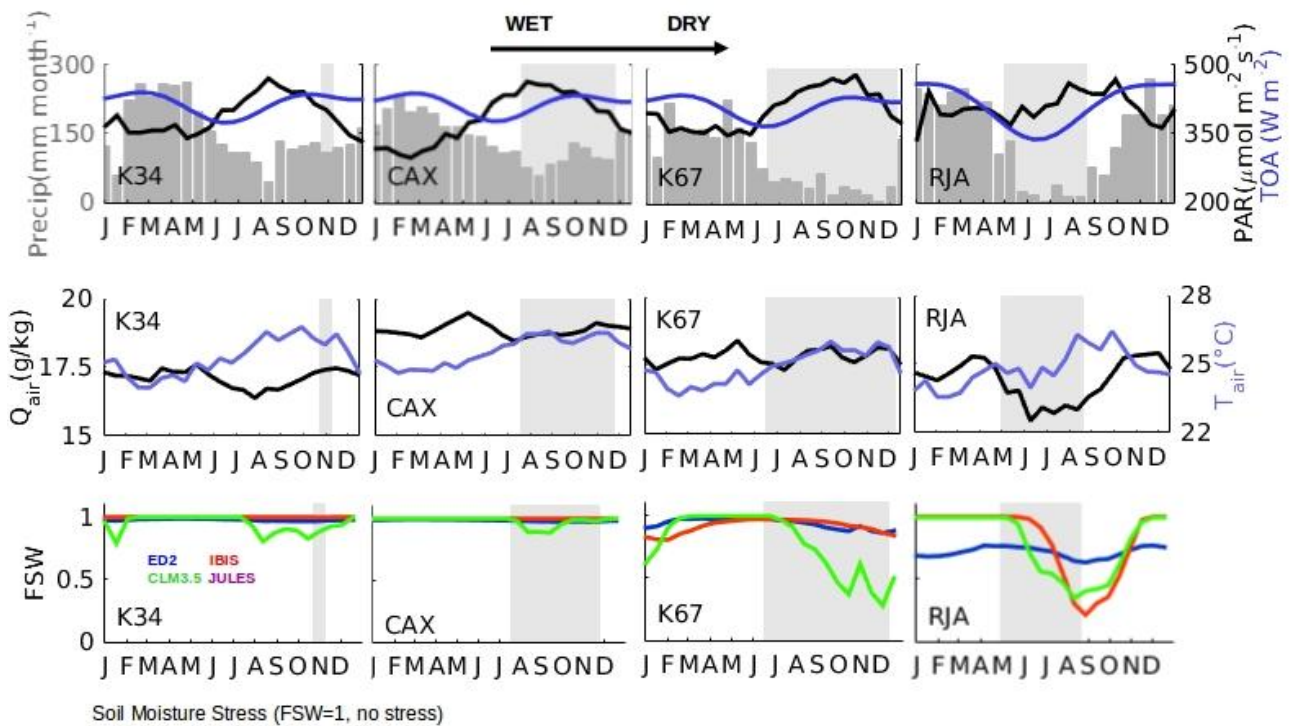
231

232 Figure 2. From top to bottom annual cycle of daily average observed climatic variables: incoming

233 photosynthetic active radiation (*PAR*; µmol m^{-2} s^{-1}, black line right y-axis) and precipitation (*Precip*;

234 mm month^{-1}, dark gray bars left y-axis), top of the atmosphere incoming radiation (*TOA*; W m^{-2},

235 blue line right y-axis) (not a driver). From left to right study sites (from wet to dry forest) near

236 Manaus forest (K34), Caxiuanã forest (CAX), Santarém forest (K67), and Reserva Jarú southern

237 forest (RJA). Gray shaded area is dry season as defined using satellite derived measures of

238 precipitation (TRMM: 1998-2014). Second row LSM drivers: near surface specific humidity (*Q$_{air}$*;

239 kg kg^{-1}, black line left y-axis) and temperature (*T$_{air}$*; °C, blue line right y-axis). Lower panel depicts

240 model ecosystem-scale of model soil moisture "stress" (*FSW*, where 1=no stress). Simulations

241 from ED2 (blue), IBIS (red), CLM3.5 (green), and JULES (purple).

242

243 From the standard suite of climatic variables available for periods between 1999 and 2006 measured

244   at each EC tower, meteorological drivers for the models were generated. Variables included:

245   SW_{down}; air temperature (T_{air}, °K); near surface specific humidity (Q_{air}, g kg^{-1}); rainfall (*Precip*, mm

246   month^{-1}); magnitude of near surface wind (WS, m s^{-1}), surface atmospheric pressure (*Pa*, hPa);

247   surface incident longwave radiation (LW_{down}, W m^{-2}); and a fixed CO_2 concentration ($CO2_{air}$ at 375

248   ppm) (de Goncalves *et al.*, 2009) (Fig. 2). Drivers were created for consecutive years where gaps

249   were no greater than two months. The data was subject to quality control and filled using other

250   tower measurements (e.g. from a temperature profile), near-by sites and the variables mean monthly

251   diurnal cycle. We analyzed data for 2000-2005 for K34, 2002-2004 for K67, 2000-2002 for RJA

252   and 1999-2003 for CAX. We restricted flux and meteorological observations and the calculation of

253   seasonality to the above-mentioned dates in order to match model drivers and output.

254

255   Hourly fluxes (*GPP, NEE, $R_{eco,}$* and *ET*) and meteorology were aggregated to 16-day time periods,

256   assuming that at least 4 days were available with at least 21 hours of observations each. Gaps were

257   not filled further and mean annual cycles were then calculated.

258

259   **2.3. Field measurements**

260   The following vegetation infrastructure descriptors and carbon pools were included on the analysis:

261   Leaf Area Index (*LAI*): model output was compared to *LAI* observations for Caxiuana, CAX as

262   reported by Metcalfe et al. (2007)), and for Santarem, K67 as by Brando et al. (2010). *LAI* was

263   normalized from 0 to 1 ($LAI_{normalized}$) for purposes of presentation. Thus, in order to visualize any

264   changes in *LAI*, independent of the observed or modeled absolute value, using Equation 1, where at

265   time *i*, LAI_i was adjusted by LAI_{min} and LAI_{max} that corresponded to the minimum and maximum

266   seasonal *LAI*, respectively:

$$LAI_{normalized(i)} = \frac{LAI_i - LAI_{min}}{LAI_{max} - LAI_{min}}$$

Equation 1

Leaf litter-fall or net primary productivity allocated to litter-fall ($NPP_{litter-fall}$, g C m^{-2} d^{-1}): values corresponded to monthly litter-bed measurements at Manaus, K34 (here presented for the first time), and to those reported by Rice et al. (2004) for K67 and by Fisher et al. (2007) for CAX.

Modeled NPP_{leaf} followed a basic leaf balance model proposed by Restrepo-Coupe et al. (2013). Assuming the change in ecosystem Pc (dPc/dt) to be driven by 1) the loss or gain of leaves, $NPP_{litter-fall}$ and NPP_{leaf}, respectively (quantity); and 2) the changes in leaf-level carbon assimilation at saturating light ($SLA \times A_{max}$) related to age (quality). Therefore, solving for leaf production we obtained:

$$NPP_{leaf} = NPP_{litter-fall} + \frac{1}{A_{max} \times SLA} \times \frac{dPc}{dt}$$

Equation 2

where specific leaf area (SLA) values were set to 0.0140 for K67 and CAX (Domingues *et al.*, 2005), 0.0164 m^2/gC for K34 (Carswell *et al.*, 2002). The A_{max} was reduced to reach 40% of the mean value at the time when leaf-fall reached its maximum (2-month linear gradient). Maximum A_{max} was set to 8.66 g C m^{-2} d^{-1} at K67 (Domingues *et al.*, 2005), and to 7.36 g C m^{-2} d^{-1} at K34 (Carswell *et al.*, 2000) and CAX.

Wood net primary productivity (NPP_{wood}) was based on stem wood increment measurements (diameter at breast height, DBH) as reported by Rice et al. (2004) at K67, Chambers et al. (2013) at K34, and da Costa et al. (2010) at CAX. No data was available for RJA.

2.4.Land system models (LSMs)

290

291   We presented output from four state-of-the-art terrestrial biosphere models. All LSMs were process

292   based (e.g. photosynthesis, respiration, and evapotranspiration) and able to simulate the fluxes of

293   carbon, water, and energy between the atmosphere and the land surface. The model simulations

294   were run as part of the Interactions between Climate, Forests, and Land Use in the Amazon Basin:

295   Modeling and Mitigating Large Scale Savannization project (Powell *et al.*, 2013).

296

297   The Ecosystem Demography model version 2 (ED2): The model explicitly tracked the dynamics of

298   fine-scale ecosystem structure and function, including net ecosystem productivity (*NEP*), carbon

299   partitioning, and growth and mortality dynamics (Medvigy *et al.*, 2009). It used four PFTs for the

300   tropics, 10-minute time step for the dynamic global vegetation model (DGVM) and *LAI* on a daily

301   basis. The number of canopy layers varied per number of plant cohorts and had three different soil

302   carbon pools for each layer (fast, slow and structural), water extraction depth varies according to

303   plant functional types (PFTs); however, the model did not included hydraulic redistribution.

304

305   The Integrated Biosphere Simulator (IBIS): The model simulated hourly carbon fluxes. *LAI* was

306   allocated annually and biomass was integrated over the year (Foley *et al.*, 1996). IBIS required 76

307   parameters to be specified, of those 14 were related to soil, 12 were specific to each of the nine

308   PFTs, and 50 were related to morphological and biophysical characteristics of vegetation.

309

310   The Community Land Model-Dynamic Global Vegetation Model version 3.5 (CLM3.5): Is the

311   predecessor to the current CLM4-CNDV model (Gotangco Castillo *et al.*, 2012), which is the land

312   component of the Community Earth System Model (CESM). CLM3.5 runs were set using a

313   prognostic phenology, which incorporated recent improvements to its canopy interception scheme,

14

314 new parameterizations for canopy integration, a TOPMODEL-based model for runoff, canopy

315 interception, soil water availability, soil evaporation, water table depth determination by the

316 inclusion of a groundwater model, and nitrogen constraints on plant productivity (without explicit

317 nitrogen cycling) (Oleson *et al.*, 2008).   The model treated the canopy as a weighted average (by

318 their respective *LAI*s) of sun and shaded leaves. The leaf phenology subroutine of this model for

319 tropical forests applied only to the Broadleaf Deciduous Tree (BDT) PFT fraction ("raingreen"

320 PFT), but all CLM3.5 simulations reported here were >95% tropical Broadleaf Evergreen Tree

321 (BET) fractional PFT cover. The allocation scheme for this model dictated that leaf turnover for the

322 tropical BET (at a rate of 0.5 yr^{-1}) be replaced instantaneously with new leaf production to maintain

323 fixed allometric relationships (Sitch *et al.*, 2003); therefore, seasonality of *LAI* was not possible for

324 these simulations.

325

326 The Joint UK Land Environment Simulator (JULES): Included a multi-layer canopy scheme for

327 light interception (built-in a sun fleck penetration scheme), a coupled scheme of leaf photosynthesis

328 and stomatal conductance, and the representation of the effects of ozone on leaf physiology. The

329 version of JULES shown here represented the carbon allocation, growth and population dynamics

330 of five plant functional types. The turnover of carbon from living plant tissues was fed into a four-

331 pool soil carbon model (Clark *et al.*, 2011).

332

333 Model output followed the LBA-Data Model Intercomparison Project (LBA-DMIP) protocol (de

334 Goncalves *et al.*, 2009); however, it includes some additional variables related to water limitation

335 (e.g. soil water availability factor or soil water "stress"), land use change (e.g. additional carbon

336 pools), and disturbance (e.g. mortality) (Powell *et al.*, 2013). Here, we present soil water "stress"

337 (*FSW*) values, calculated following Ju et al. (2006). By definition *FSW* ranging from 0 to 1 is a

338 measure of the water available to roots, where $FSW=1$, is no stress.

339

340 **3.   Results**

341 **3.1. Gross primary productivity (GPP) and ecosystem photosynthetic capacity (Pc)**

342 The observed annual cycle of ecosystem-scale GPP showed two divergent patterns: (1) increasing

343 levels of photosynthetic activity (GPP) as the dry season progresses in the equatorial Amazon (K34,

344 K67 and CAX) where $MiAP$ was 60 and 36 mm month^{-1}, respectively, and maximum radiation was

345 synchronous with low precipitation; and (2) declining productivity as the dry-season advanced in

346 the southern forests (RJA) where radiation was somewhat aseasonal and $MiAP$ was less than half its

347 central Amazon counterparts (14 mm month^{-1}) (Fig. 1). By contrast, at all sites, model simulations

348 showed peak GPP seasonality at the end of wet season with declining GPP during the dry season

349 (Fig. 3). The reduced dry season GPP observed at the southern Amazon forest of Jarú (RJA) was

350 consistent with increasing degrees of water limitation. At the sites in the equatorial Amazon (K34,

351 K67 and CAX), modeled soil water "stress" (FSW; Fig. 2) (where $FSW=1$, no stress) acted to

352 reduce model GPP during the dry season, even as observed Pc increased following higher levels of

353 incoming solar radiation (PAR; Fig. 2 and Pc; Fig. 4). Similar to GPP, models tended to achieve

354 good Pc representation at RJA. However, simulated Pc at the equatorial Amazon forest sites

355 remained unchanged (IBIS and JULES) or decreasing gradually from the middle of the wet season

356 to the end of the dry period at K67 (ED2 and CLM3.5) (Fig. 4).

357

358

16

359
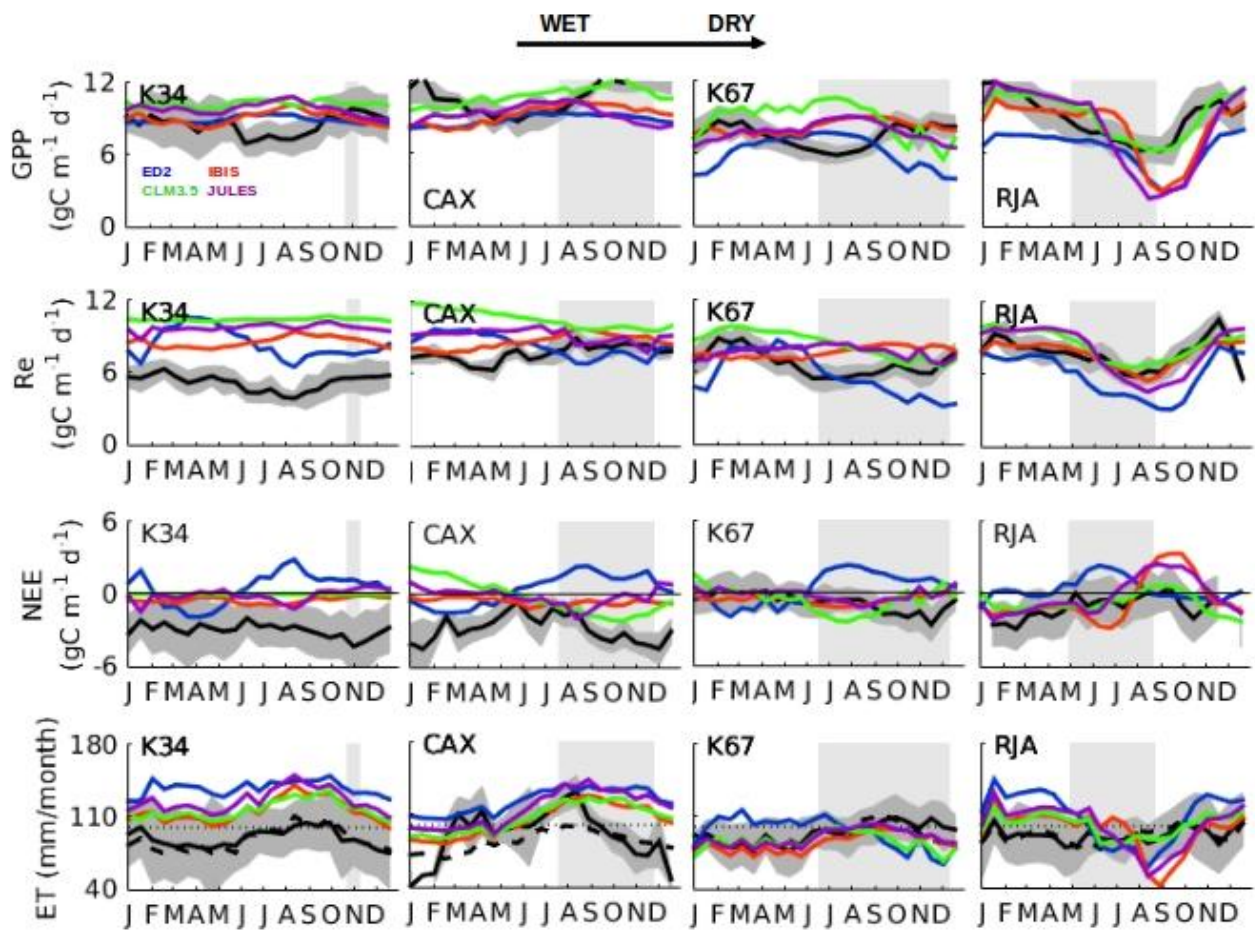
Figure 3: Annual cycle of daily average ecosystem-scale photosynthesis (GPP; $gC\,m^{-2}\,d^{-1}$),

ecosystem respiration (R_e; $gC\,m^{-2}\,d^{-1}$) net ecosystem exchange (NEE; $gC\,m^{-2}\,d^{-1}$) and

evapotranspiration (ET; $mm\,d^{-1}$) near Manaus forest (K34), Caxiuanã forest (CAX), Santarém forest

(K67), and Reserva Jarú southern forest (RJA). Observed (black + dark gray uncertainty) and

simulated by models (colors). Dashed black line at ET panels corresponds to a linear model where

the independent variable is incoming radiation (SW_{down}). Gray shaded area is dry season as defined

using satellite derived measures of precipitation (TRMM: 1998-2014). Simulations from ED2

(blue), IBIS (red), CLM3.5 (green), and JULES (purple). Observations from the Brasil flux network.

368

FSW reached an all-site minimum at RJA by the end of the dry season (Fig. 2) and corresponded

with a decrease in model *ET* not seen on the EC measurements (Fig. 3). With the exception of CAX,

17

371 seasonal observations of *ET* at all of the sites showed very little seasonality and remained close to

372 120 mm month^{-1} (4 mm d^{-1}). In general, models were able to capture the seasonality of *ET*;

373 however, they overestimated the dry-period reduction in water exchange at RJA and in the case of

374 K34 and CAX overestimated *ET* absolute values. By contrast, a very simple linear regression

375 driven by *SW$_{down}$* was able to represent ~83% of the seasonality of *ET* (Fig. 3).

376

377   **3.2 Carbon allocation**

378 We explored different model approaches to simulate the phenology of carbon allocation, in

379 particular measures of plant metabolism (ecosystem photosynthetic capacity, *Pc* as proxy), standing

380 biomass (wood increment, leaf-production and the balance of gain and loss of leaves), and additions

381 to soil organic matter (leaf-fall), in an attempt to understand the model-data discrepancies on the

382 estimates of *GPP* and *NEE*.

383

384 Our results indicated that none of the models was able to capture or replicate the observed dry-

385 season *LAI* changes at our equatorial Amazon forests EC locations (Fig. 4). In addition, with the

386 exception of ED2, the annual mean *LAI* values were unrealistically high (Baldocchi *et al.*, 1988;

387 Gower *et al.*, 1999; Asner *et al.*, 2003; Sakaguchi *et al.*, 2011). In contrast, with some model

388 phenology schemes that assumed *LAI* and *T$_{air}$* to be positively correlated, we observed a negative o

389 no correlation (non-statistically significant; p-value >0.1) (Supplement Fig. 6).

390

391 In the field, leaf litter-fall plays an important role in determining the seasonality of *LAI*, *Pc* (as per

392 Equation 2), heterotrophic respiration and soil carbon pools. Data for the central Amazon forests

393 showed a highly seasonal leaf-fall cycle (Chave *et al.*, 2010), with an *LAI* maximum at the

394 beginning of the dry season at CAX and in the middle of the dry period at K67 (Fig. 4). At

395 equatorial sites, peak litter-fall corresponded to a maximum in SW_{down}, where we observed a

396 statistically significant linear regression between SW_{down} and $NPP_{litter-fall}$ with a coefficient of

397 determination, R^2 equal to 0.34 at K34, 0.21 at K67, and 0.6 at CAX (p<0.01) (Supplement Fig. 2).

398 With the exception of ED2, which included a drought-deciduous phenology and consequentially

399 seasonal variations in leaf abscission, seasonality in $NPP_{litter-fall}$ was not resolved in most LSMs (Fig.

400 4).

401

402 Estimates of leaf-production (increase in the amount of young-high photosynthetic capacity leaves)

403 from the observations at K67 forest showed peak NPP_{leaf} in the dry season in contrast to most

404 simulations. In general, NPP_{leaf} was: (1) constant in most models; (2) allocated at the end of the

405 year, similar to $NPP_{liter-fall}$; or (3) declining, in particular during the strong K67 dry season (Fig. 2).

406 Even if counterintuitive, at some of the equatorial Amazon sites key leaf-demography processes

407 (e.g. leaf-fall and leaf-flush) and/or LAI, increased in tandem during the dry season.

408

409 In contrast to NPP_{leaf}, NPP allocation to wood growth (NPP_{wood}) was aseasonal at K34; however at

410 K67 peaked during the wet season, displaying opposite seasonality and being out-of-phase with

411 NPP_{leaf}. This pattern seemed to be different at CAX, with both NPP_{leaf} and NPP_{wood} maximum

412 during the dry season, at this site precipitation was significantly seasonal (wet season was the

413 rainiest of all equatorial sites) and the amplitude of the seasonal cycle of SW_{down} was the highest of

414 all Brasil flux central Amazon locations. By contrast, models simulated a peak in NPP_{wood} at CAX

415 and K67 that corresponded to the beginning of the dry season. The seasonality of model NPP_{wood}

416 was absent at the three equatorial forests and only significant differences between the wet and dry

417 periods were observed at RJA, where all simulations showed minimum NPP_{wood} at the end of the

418 dry season.
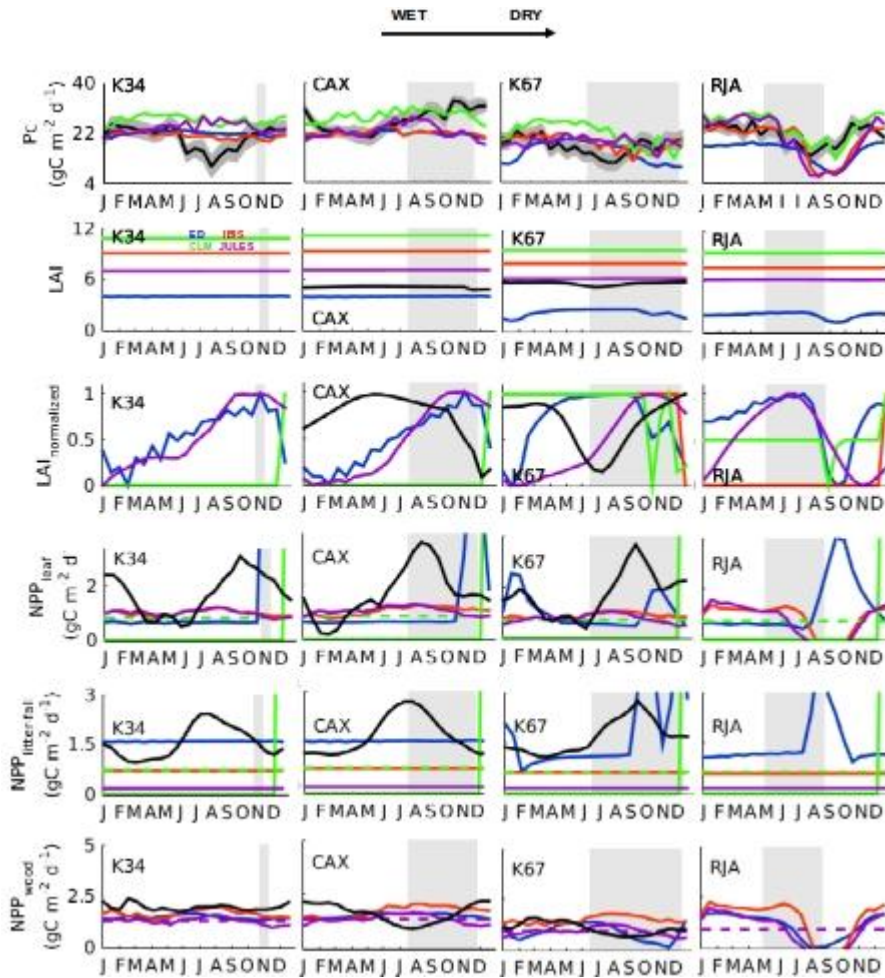
419

420   Figure 4. From top to bottom annual cycle of daily average ecosystem photosynthetic capacity (*Pc*,

421   *GPP* at a fixed *PAR* range 725-875 µmol m^{-2} s^{-1}, Leaf Area Index (*LAI; m m^{-1}*), normalized *LAI* (its

422   value constrained between 0 and 1 in order to better track its changes), net primary productivity

423   (*NPP; m^{-2} d^{-1}*) allocated to leaves -leaf flush (*NPP$_{leaf}$*; m^{-2} d^{-1}), *NPP* allocated to litter-fall (*NPP$_{litter-}$*

424   *$_{fall}$*; gC m^{-2} d^{-1}). Gray shaded area is dry season as defined using satellite derived measures of

425   precipitation (TRMM: 1998-2014). Lower row *NPP* allocated to wood (*NPP$_{wood}$*; gC m^{-2} d^{-1}).

426   From left to right study sites (from wet to dry forest) near Manaus forest (K34), Caxiuanã forest

427   (CAX), Santarém forest (K67), and Reserva Jarú southern forest (RJA). Observed (black) *versus*

428   simulated by models (colors). Simulations from ED2 (blue), IBIS (red), CLM3.5 (green), and

429   JULES (purple). Dashed green lines (CLM3.5) at *NPP$_{litter-fall}$* and *NPP$_{leaf}$*, indicate average values

430   for comparison purposes (models allocated at the end of the year as indicated by continuous line).
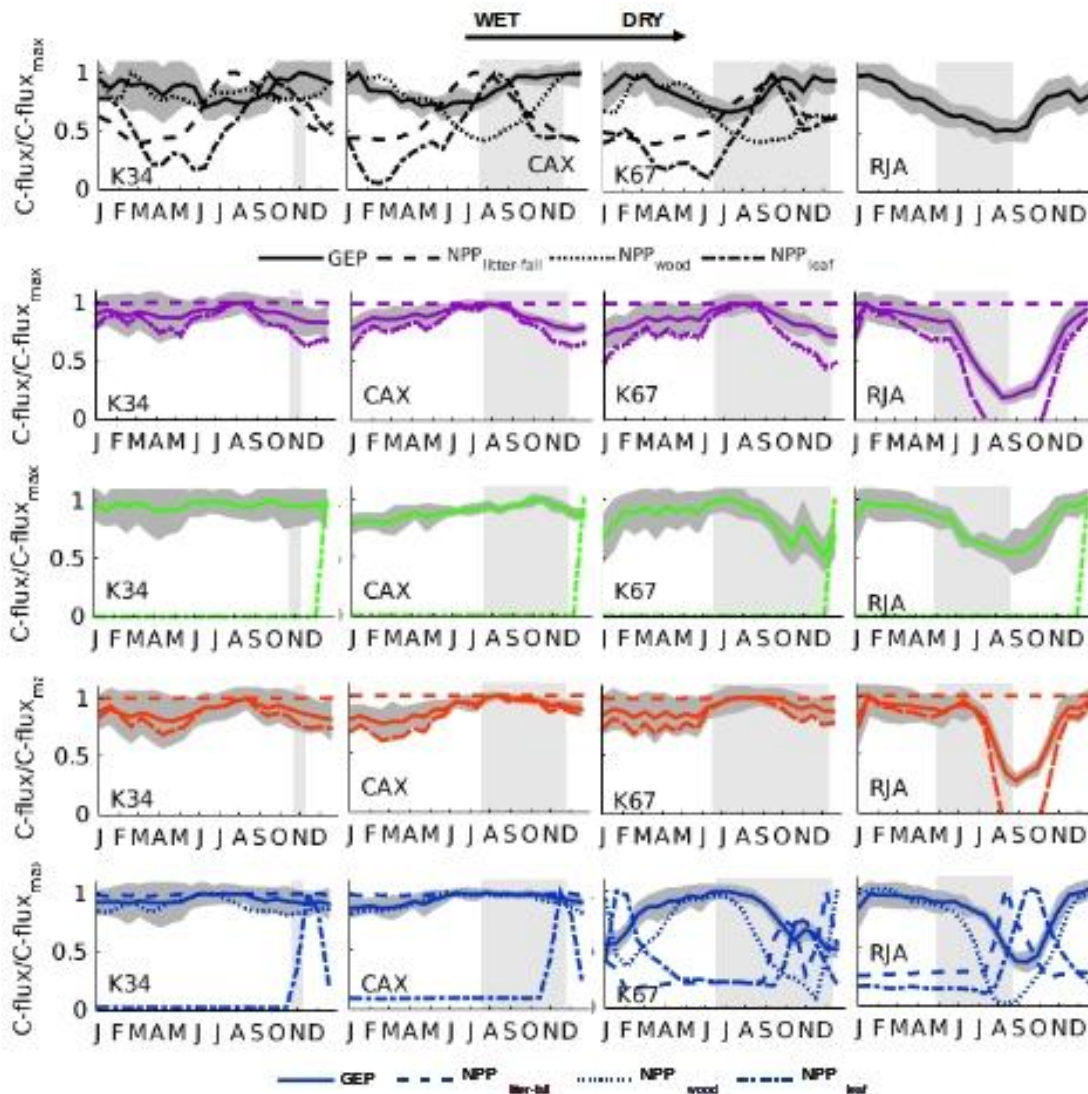
Figure 5. From left to right study sites (from wet to dry forest) near Manaus forest (K34), Caxiuanã forest (CAX), Santarém forest (K67), and Reserva Jarú southern forest (RJA). From top to bottom, annual cycle observed (black) and model simulations from JULES (purple), CLM3.5 (green), IBIS (red), and ED2 (blue). Normalized (by its seasonal maximum) annual cycle of daily average ecosystem-scale photosynthesis (GPP/GPP_{max}) (continuous line), net primary productivity (NPP) allocated to leaves -leaf flush ($NPP_{leaf}/NPP_{leaf\,max}$), NPP allocated to litter-fall ($NPP_{litter\text{-}fall}/NPP_{litter\text{-}fall\,max}$), and NPP allocated to wood ($NPP_{wood}/NPP_{wood\,max}$). Gray shaded area is dry season as defined using satellite derived measures of precipitation (TRMM: 1998-2014).

441

442 Our analysis shows a statistically significant negative linear regression between SW_{down} and NPP_{wood}

443 with a coefficient of determination, R^2 equal to 0.45 at K67 and 0.62 at CAX (p<0.01) (Supplement

444 Fig. 3). Non-significant correlation was found between SW_{down} and NPP_{wood} or precipitation and

445 NPP_{wood} at K34 -the wettest and least seasonal of the four studied forests.

446

447 Seasonal observations of the different NPP components and GPP showed a lack of temporal

448 synchrony between them, neither a shared allocation pattern among forests –each exhibiting

449 different phenology (Fig. 5). At some sites (CAX and K67), there was a statistically significant

450 correlation (~1 to 2-month lag, NPP_{leaf} ahead) between GPP and NPP_{leaf} (Supplement Fig. 5).

451 However, there was no temporal correspondence between GPP and NPP_{wood}. By comparison,

452 model allocation (NPP_{leaf}, $NPP_{litter-fall}$ and NPP_{wood}) and GPP was coupled at most models (Fig. 5).

453

454 **3.2 Ecosystem respiration (R_e) and net ecosystem exchange (NEE)**

455 Similar to GPP, the timing and amplitude of ecosystem respiration (R_e) seasonality at RJA was well

456 captured by most models; however, all simulations at equatorial Amazon sites overestimated R_e. In

457 particular, during the months for which R_e reached a minimum -the wet season at CAX and the dry

458 season at K67, model R_e showed opposite seasonality to observations. The imbalance between

459 predicted R_e and GPP translated into an underestimation of the observed net ecosystem uptake

460 (negative NEE), with the models predicting a positive NEE (strong carbon source), in particular, at

461 K34 and CAX. More importantly, the seasonality of NEE in the equatorial forests (K34, K67 and

462 CAX) was missed, with the LSMs foreseeing a greater carbon loss during the dry season, as

463 opposed to those observed during the September-December losses (Fig. 3).

464

465 ## 4. Discussion

466 In this study, we found that land surface models poorly represented the annual cycle of carbon flux

467 dynamics for the Amazon evergreen tropical forest sites with eddy covariance towers. In particular,

468 at equatorial Amazonia, observations showed an increase in *GPP*, *Pc*, and/or *LAI* during the dry

469 season. In contrast, models simulated constant or declining *GPP* and *Pc*, and in general, assumed

470 no seasonal cycling in *LAI* (Fig. 4). The disparity between model and *in situ* measurements of *GPP*

471 indicated that there is a bias in the modeled ecosystem response to climate and a lack of

472 understanding of which drivers, meteorological (e.g. light or water) or phenological (e.g. leaf

473 demography) or a combination thereof, control ecosystem carbon flux. Moreover, a mismatch

474 between seasonal observations of carbon pools and allocation strategies (NPP_{leaf}, NPP_{wood}, $NPP_{litter-}$

475 $_{fall}$) and model results, highlights the importance of phenology as an essential tool for understanding

476 productivity within the tropical forest of the Amazon.

477

478 ### 4.1 Seasonality of gross primary productivity (*GPP*), and other carbon fluxes

479 We observed the greatest discrepancies between measured and model predicted *GPP*, R_e, and *NEE*

480 at central Amazon sites, where productivity is hypothesized to be primarily controlled by a

481 combination of light availability and phenology (Wu *et al.*, submitted; Restrepo-Coupe *et al.*, 2013).

482 By contrast, models were able to capture the "correct" seasonality at the southern forest of RJA, a

483 site that shows significant signs of water limitation. However, at RJA the amplitude of the annual

484 cycle were overestimated by most models, which assume lower than expected *GPP* during the dry

485 season. Our results suggest that, while models have improved their ability to simulate water stress;

486 their ability to simulate light-based growth strategies is still an issue.

487

488 Satellite phenology studies have shown annual precipitation values and the length of the dry season

489 to be important factors when determining ecosystem response (Guan *et al.*, 2015). Nevertheless,

490 K67 and RJA share similar rainfall values, with *MAP* of 2030 mm year^{-1}, dry season precipitation

491 (*DSP*) of 50 mm month^{-1}, and a 4 to 5 month dry period, only the minimum annual precipitation

492 differs, having RJA *MiAP* of 14 compared to 37 mm month^{-1} measured at K67. Moreover,

493 increasing levels of incoming light at K67 and other equatorial sites during the dry season provided

494 an opportunity for vegetation to increase productivity under the existent precipitation regime, as

495 rainfall delivered more than 50% of ecosystem water needs assuming a monthly ~120 mm

496 requirement. For central Amazon tropical forests, observed increases in *GPP*, vegetation

497 photosynthetic potential (*Pc* as a proxy), and allocation patterns, linked to light harvesting strategies,

498 were concurrent with the reported incoming in solar radiation increase (Huete *et al.*, 2006; Brando

499 *et al.*, 2010; Restrepo-Coupe *et al.*, 2013). By comparison, at RJA, there was no tradeoff between

500 light, precipitation and atmospheric demand, as solar radiation was somewhat aseasonal (with a

501 maximum at the beginning of the wet season) and dry season rainfall values (*MiAP*) reached less

502 than 10% of mean tropical forest *ET*.

503

504 **4.2 Carbon allocation strategies**

505 Models include *LAI* in the vegetation dynamics module using a variety of strategies: (1) prescribed

506 *LAI* values from remote sensing sources; (2) dynamic calculation of daily *LAI;* and (3) *LAI* is fixed

507 and the model later allocating any changes at the end of the year, thus only to calculate changes in

508 the carbon balance and next year *LAI* values. This last approach may need to be re-evaluated given

509 the importance of phenology as an ecosystem productivity driver. Models that dynamically

510 calculate *LAI* generally rely in defining *LAI* range values for each PFT (Clark *et al.*, 2011), where

511 the actual value will depend mostly on the phenological status of the vegetation type –a function of

512 temperature. Although some evergreen ecosystems do respond to temperature thresholds (e.g.

513 positive correlation between T_{air} and LAI and a threshold at T_{air}>0 has been identified for conifer

514 forests at temperate areas (Khomik *et al.*, 2010)), LAI and Pc at tropical ecosystems do exhibited a

515 negative or no correlation with T_{air}. Moreover, model LAI values were unreasonably 2+ units above

516 observed values (Baldocchi *et al.*, 1988; Gower *et al.*, 1999; Asner *et al.*, 2003; Sakaguchi *et al.*,

517 2011). Some models assumed LAI value above six, the theoretical limit of LAI (assuming no

518 clumping and planar leaf angle distribution) according to Beer's law. Similar to previous findings

519 by Christoffersen et al. (2014) regarding model performance when simulating water fluxes, some of

520 the model deficiencies could be resolved by changing the parameterization of each PFT, such as the

521 case of maximum and minimum LAI values. However, a true improvement will only come if we

522 increase the frequency and coverage of our measurements, and a better understanding of the carbon

523 allocation, mechanisms that control the change in LAI, and the balance between loss due to

524 abscission, leaf production, and other ecosystem processes.

525

526 In the observations, Pc values increased during the dry season at all central Amazon sites. Elevated

527 Pc can be achieved through leaf flush, as younger leaves have higher leaf carbon assimilation at

528 saturating light (A_{max}) compared to old leaves (Wu *et al.*, submitted; Sobrado, 1994), or by changes

529 in leaf herbivory, *epiphyllous* growth, and stress, among other factors. Alternatively, Pc can be

530 increased through a surge in canopy infrastructure (quantity of leaves) measured as leaf area index

531 (LAI) (Doughty & Goulden, 2008). Our observations suggested a combination of these two

532 processes or Pc mostly driven by the presence of younger leaves, as we observed a small increase in

533 LAI at K67 during the dry season (0.7 m^2/m^2 ~10% of annual mean) and a gradual decline at CAX,

534 respectively. In order to address the relationship between leaf demography (leaf age distribution)

535 and carbon fluxes, we presented the seasonality of *in situ* observations of NPP_{leaf} and compared it to

536 model estimates. We have shown that, at the equatorial Amazon estimated NPP_{leaf} was

537 synchronous with the seasonality of SW_{down}. Thus, increasing light may trigger new leaf production

538 as part of a light-based growth strategy missed by the models evaluated here. Some vegetation

539 schemes have introduced a time-dynamic carbon allocation: to leaves, generic roots, coarse and fine

540 roots, etc. However, even if models assign NPP_{leaf} varying turnover time from 243 days to a

541 maximum of 2.7 years, the timing of leaf production seems to be missed. The counterintuitive

542 mechanism observed at some central Amazon forests where all or most of the leaf-demography

543 processes (leaf-fall, leaf-flush and LAI) increase during the dry season, constitutes an important

544 challenge for modelers and plant physiologists. An appropriate model representation and further

545 studies are required of: (1) the leaf lifespan, (2) the seasonality of leaf age distribution (e.g. sun and

546 shade leaf cohorts: young, mature, old), (3) the effect of leaf-fall on increasing light levels at lower

547 layers of the canopy, and (4) the relationship between leaf age and physiology (Albert *et al.*, in

548 preparation), to properly characterize Amazon basin leaf phenology and associated changes in

549 productivity. Thus, as a homogeneous age cohort where all leaves have similar ability to assimilate

550 carbon can contribute to the model simulated aseasonal Pc and GEP seasonality driven only by

551 water availability.

552

553 Previous studies have linked the robustness of models predictions of the terrestrial ecosystem

554 carbon response to climate change projections to the uncertainty of the different carbon pools within

555 the models (Ahlström *et al.*, 2012). Observations show that the seasonality of allocation (e.g.

556 $NPP_{litter-fall}$) and leaf-demography (e.g. NPP_{leaf}) are closely related to the fast and slow soil carbon

557 pools (input) and ecosystem respiration. Decomposition of $NPP_{litter-fall}$ initiates the transfer of

558 carbon to the soil microbial and the slow and passive pools in many models and determines

559 heterotrophic respiration. Similarly, autotrophic respiration (maintenance and growth) also will be

560 driven by live tissue allocation (NPP_{wood}, NPP_{leaf}, and NPP_{roots}). Therefore, R_{eco} will depend on a

561 well-characterized phenological response of litter and woody debris, wood and leaf accumulation,

562 and the soil carbon pools. Still, in some models and according to a set of prescribed allometric

563 relationships for each PFT where leaves, fine roots and stems NPP are allocated at the end of each

564 simulated year. Thus, to improve simulation-data agreement and to generate reliable projections for

565 ecosystem response to climate perturbations, the next generation of models must include a basic

566 mechanistic understanding of the environmental controls on ecosystem metabolism that goes

567 beyond correlations (e.g. NPP_{leaf} versus SW_{down}, $NPP_{litter\ fall}$ versus $Precip$) and addresses the long

568 time adaptation to climate and their seasonality. We highlight the need for extended EC

569 measurements accompanied by seasonal based biophysical inventories, as both datasets

570 complement and inform each other.

571

572 The seasonal patterns in seasonal GPP and NPP (leaf and wood); show to be (1) aseasonal at K34;

573 (2) synchronous at CAX; and (3) out-of-phase at K67. The GPP, NPP_{leaf} and NPP_{wood} dry-season

574 maxima at CAX may be interpreted in terms of a combination of mechanisms: (1) optimal

575 allocation patterns (Doughty et al., 2014) -- in sync photosynthetic activity and carbon allocation

576 driven by dry-season light increases; and (2) reflect biophysical limitations (Fatichi et al., 2014) --

577 wet season anoxia, drive both leaves and wood to be produced during the dry season. Similar to

578 CAX, observations of a simultaneous increase in NPP_{leaf} and NPP_{wood} during the dry season have

579 been reported at seasonally inundated floodplain tropical forests, where anoxia limits respiratory

580 requirements of NPP_{wood} and show peak NPP_{wood} shifted into the dry season (Dezzeo et al., 2003).

581 Consistently, seasonal observations at flooded forests showed reduced production of new leaves and

582 lower photosynthetic assimilation during the inundation period (Parolin, 2000). By comparison, the

583 NPP_{wood} patterns observed at K67 where dry-season $MiAP$ is ~50% of mean annual ET may reflect

584 biophysical limitations on the sink tissue (e.g. cell turgor and cell division in cambial tissues) --

585 water availability as a driver (Wagner *et al.*, 2012; Rowland *et al.*, 2013), or/and an allocation

586 strategy that favors NPP_{leaf} to NPP_{wood}. At K67 and K34 forests, the timing of GPP *versus* NPP_{wood}

587 highlights the importance of NSC (Fatichi *et al.*, 2014) and difficulties faced by more mechanistic

588 LSMs.

589
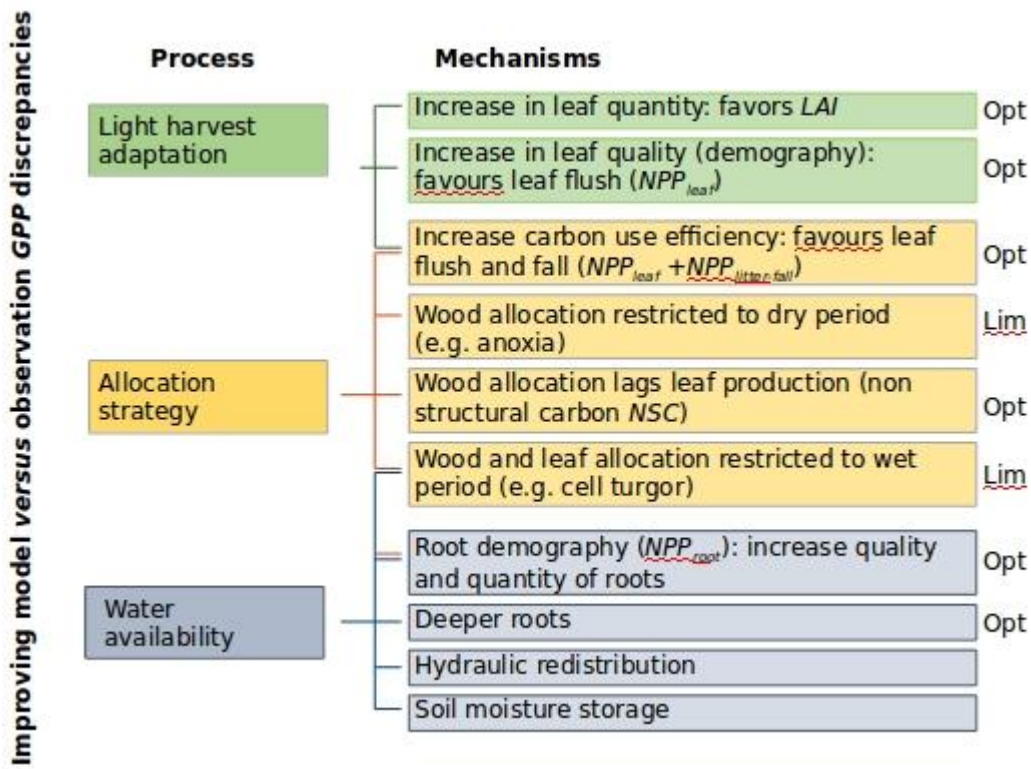
Figure 6. Ecosystem response to climate seasonality □ selection of biological adaptive mechanisms:

591 light harvest adaptations (green tones), allocation strategies (orange tones), and water limitation

592 (blue tones). Mechanisms classified when possible into resource optimization (Opt) and biophysical

593 limitations (Lim).

594

4.3 Final considerations for model improvement

596 This study identified three main tropical forest responses to climatic drivers that if understood could

597 reduce the model – observation GPP discrepancies. These are (1) light harvest adaptation schemes;

598 (2) response to water availability; and (3) other allocation strategies (Fig. 6). We propose thorough

599   (1) optimization patterns and (2) thresholds (limitation) to obtain the seasonality of the different

600   carbon pools. For example, models could incorporate some of the recent findings: (1) leaf

601   demography as a function of light environment as in Wu et al. (submitted), and (2) leaf phenology

602   (greenness) seasonal patterns driven by soil moisture availability as a function of MAP threshold as

603   in Guan et al. (2015). However, less has been reported about other processes and reservoirs

604   different than NPP_{leaf}. In particular, our study lacks belowground information, as data that explores

605   the seasonality of root allocation at tropical sites is scarce and difficult to interpret. Future work

606   should address this important carbon-pool and the correspondent model ability to simulate the

607   seasonality of belowground processes.

608

609   Climate models have come a long way, from the 1970 when the first land surface scheme was

610   introduced in order to represent the atmosphere-biosphere interaction by partitioning ocean from

611   dry land (Manabe & Bryan, 1969). Simulations of water, energy and carbon fluxes based on the

612   response of different plant functional types to climate drivers and disturbance signifies a great step

613   forward on weather prediction and the study of future climates under the effect of land cover

614   changes and atmospheric CO_2 enrichment (Pitman, 2003; Niu & Zeng, 2012). Models are

615   constrained in their development given the high computational needs and the multiple processes

616   that need to be accounted for on a three dimensional grid from LAI seasonality, to ground water flux,

617   to leaf level parameterization, there is a tradeoff and a "priority list". This study highlights some of

618   the advances in tropical forest simulations of carbon and water fluxes and aims to identify future

619   opportunities, as the inclusion of light harvesting and allocation strategies in an attempt to improve

620   GPP and NPP predictions.

621

622 **5.   Conclusions**

623 At central Amazon tropical forests, four land surface models (LSMs) simulated gross primary

624 productivity (*GPP*) peaks at the end of wet season, and then declines along with the progress of the

625 dry season, thus in contrast to eddy covariance observations, which reach a minimum *GPP* at end of

626 wet season and then increase in the dry season. Similarly, the modeled annual cycle of daily

627 average ecosystem-scale respiration (R_e) and net exchange (*NEE*) was out-of-phase and their

628 absolute values were overestimated for R_e and underestimated for *NEE*. The above-mentioned

629 discrepancies between predicted and observed carbon fluxes indicate that some models may be

630 missing important processes. Our work highlights phenology, allocation strategies, and plant

631 physiological responses to seasonal climatic constraints (i.e. low light and water availability) as

632 important descriptors of ecosystem photosynthetic capacity (*Pc*), and thus, key drivers of ecosystem

633 productivity and other metabolic processes (e.g. heterotrophic respiration). Interestingly, water

634 limitation issues previously reported seem to be resolved by most models, as seen by improvements

635 on the simulation of ecosystem *ET*.

636

637 We explore different ESM approaches to track the phenology of carbon allocation, in particular

638 measures of plant metabolism (*Pc* as proxy), standing biomass (wood increment and leaf-flush) and

639 additions to soil organic matter (leaf-fall) in an attempt to understand the model-data discrepancies

640 on the estimates of *GPP* and *NEE*. We are able to identify the seasonality of net primary

641 productivity allocated to litter-fall (*NPP_{litter-fall}*) and leaf production (*NPP_{leaf}*) and the total balance

642 (leaf area index, *LAI*) as key biological drivers, which if understood (mechanisms and vegetation

643 response) and properly implemented, could improve model predictions. In particular, *in situ*

644 observations show that at the central Amazon estimated *NPP_{leaf}* is synchronous with the seasonality

645 of incoming solar radiation, a light-based growth strategy missed by most of models. Similarly, the

646   seasonality of *LAI* at tropical forests seems underestimated and the mechanisms that control the

647   change in *LAI* and the balance between loss of capacity due to $NPP_{litter-fall}$ and increase of capacity

648   from NPP_{leaf}, not well understood. The counterintuitive leaf-demography process observed at some

649   equatorial Amazon sites ($NPP_{litter-fall}$ versus NPP_{leaf}) where Pc and/or *LAI* increased during the dry

650   season, and the here reported lags between *GPP* and NPP_{wood}, challenge Amazon basin model

651   phenology representations. As fluxes are not exclusively driven by meteorology, incorporating this

652   key biological adaptive mechanisms into ESMs is an important task in order to advance our

653   understanding of tropical vegetation-climate feedbacks.

654

666

667   **References**

Ahlström A, Schurgers G, Arneth A, Smith B (2012) Robustness and uncertainty in terrestrial

       ecosystem carbon response to CMIP5 climate change projections. *Environmental Research*

Letters, **7**, 1–9.

Ahlström A, Raupach MR, Schurgers G et al. (2015) The dominant role of semi-arid ecosystems in the trend and variability of the land CO2 sink. *Science*, **348**, 895–899.

Albert L, Restrepo Coupe N, Christoffersen B et al. (in preparation) Global implications of hidden seasonality: Amazon evergreen forests as a case study in cryptic phenology. *Plant Physiology*.

Araújo AC, Nobre AD, Kruijt B et al. (2002) Comparative measurements of carbon dioxide fluxes from two nearby towers in a central Amazonian rainforest: The Manaus LBA site. *Journal of Geophysical Research*, **107**, LBA 58–1–LBA 58–20.

Asner GP, Scurlock JMO, A. Hicke J (2003) Global synthesis of leaf area index observations: implications for ecological and remote sensing studies. *Global Ecology and Biogeography*, **12**, 191–205.

Baker IT, Prihodko L, Denning AS, Goulden M, Miller S, Rocha HR da (2008) Seasonal drought stress in the Amazon: Reconciling models and observations. *Journal of Geophysical Research*, **113**, 1–10.

Baldocchi DD, Hincks BB, Meyers TP (1988) Measuring Biosphere-Atmosphere Exchanges of Biologically Related Gases with Micrometeorological Methods. *Ecology*, **69**, 1331–1340.

Betts RA, Cox PM, Collins M, Harris PP, Huntingford C, Jones CD (2004) The role of ecosystem-atmosphere interactions in simulated Amazonian precipitation decrease and forest dieback under global climate warming. *Theoretical and Applied Climatology*, **78**, 157–175.

Brando PM, Goetz SJ, Baccini A, Nepstad DC, Beck PSA, Christman MC (2010) Seasonal and interannual variability of climate and vegetation indices across the Amazon. *Proceedings of the National Academy of Sciences of the United States of America*, **107**, 14685–14690.

Carswell FE, Meir P, Wandelli EV et al. (2000) Photosynthetic capacity in a central Amazonian

rain forest. *Tree Physiology*, **20**, 179–186.

Carswell FE, Costa AL, Palheta M et al. (2002) Seasonality in CO2 and H2O flux at an eastern

    Amazonian rain forest. *Journal of Geophysical Research*, **107**, LBA 43-1–LBA 43-16.

Castanho ADA, Coe MT, Costa MH, Malhi Y, Galbraith D, Quesada CA (2013) Improving

    simulated Amazon forest biomass and productivity by including spatial variation in

    biophysical parameters. *Biogeosciences*, **10**, 2255–2272.

Chambers JQ, Pereira da Silva R, Pereira da Silva E, dos Santos J, Higuchi N (2013) LBA-ECO

    CD-08 Tree Diameter Measurements, Jacaranda Plots, Manaus, Brazil: 1999-2001.

Chave J, Navarrete D, Almeida S et al. (2010) Regional and seasonal patterns of litterfall in tropical

    South America. *Biogeosciences*, **7**, 43–55.

Christoffersen BO, Restrepo-Coupe N, Arain MA et al. (2014) Mechanisms of water supply and

    vegetation demand govern the seasonality and magnitude of evapotranspiration in Amazonia

    and Cerrado. *Agricultural and Forest Meteorology*, **191**, 33–50.

Clark DB, Mercado LM, Sitch S et al. (2011) The Joint UK Land Environment Simulator (JULES),

    model description – Part 2: Carbon fluxes and vegetation dynamics. *Geosci. Model Dev.*, **4**,

    701–722.

da Costa ACL, Galbraith D, Almeida S et al. (2010) Effect of 7 yr of experimental drought on

    vegetation dynamics and biomass storage of an eastern Amazonian rainforest. *New*

    Phytologist, **187**, 579–591.

Cox PM, Pearson D, Booth BB, Friedlingstein P, Huntingford C, Jones CD, Luke CM (2013)

    Sensitivity of tropical carbon to climate change constrained by carbon dioxide variability.

    Nature, **494**, 341–344.

Delbart N, Ciais P, Chave J, Viovy N, Malhi Y, Le Toan T (2010) Mortality as a key driver of the

    spatial distribution of aboveground biomass in Amazonian forest: results from a dynamic

vegetation model. *Biogeosciences*, **7**, 3027–3039.

De Weirdt M, Verbeeck H, Maignan F et al. (2012) Seasonal leaf dynamics for tropical evergreen

forests in a process-based global ecosystem model. *Geosci. Model Dev.*, **5**, 1091–1108.

Dezzeo N, Worbes M, Ishii I, Herrera R (2003) Annual tree rings revealed by radiocarbon dating in

seasonally flooded forest of the Mapire River, a tributary of the lower Orinoco River,

Venezuela. *Plant Ecology*, **168**, 165–175.

Domingues TF, Berry JA, Martinelli LA, Ometto JPHB, Ehleringer JR (2005) Parameterization of

Canopy Structure and Leaf-Level Gas Exchange for an Eastern Amazonian Tropical Rain

Forest (Tapajós National Forest, Pará, Brazil). *Earth Interactions*, **9**, 1–23.

Doughty CE, Goulden ML (2008) Seasonal patterns of tropical forest leaf area index and CO2

exchange. *Journal of Geophysical Research*, **113**, 1–12.

Doughty CE, Malhi Y, Araujo-Murakami A et al. (2014) Allocation trade-offs dominate the

response of tropical forest growth to seasonal and interannual drought. *Ecology*, **95**, 2192–

2201.

Eltahir E a. B, Bras RL (1994) Precipitation recycling in the Amazon basin. *Quarterly Journal of

the Royal Meteorological Society*, **120**, 861–880.

Eva HD, Huber (eds) O (2005) A Proposal for Defining the Geographical Boundaries of Amazonia:

Synthesis of the results from an Expert Consultation Workshop organized by the European

Commission in collaboration with the Amazon Cooperation Treaty Organization - JRC Ispra,

7-8 June 2005.

Fatichi S, Leuzinger S, Körner C (2014) Moving beyond photosynthesis: from carbon source to

sink-driven vegetation modeling. *New Phytologist*, **201**, 1086–1095.

Fisher RA, Williams M, Costa D et al. (2007) The response of an Eastern Amazonian rain forest to

drought stress: results and modelling analyses from a throughfall exclusion experiment.

34

Global Change Biology, **13**, 2361–2378.

Foley JA, Prentice IC, Ramankutty N, Levis S, Pollard D, Sitch S, Haxeltine A (1996) An integrated biosphere model of land surface processes, terrestrial carbon balance, and vegetation dynamics. *Global Biogeochemical Cycles,* **10**, 603–628.

Friedlingstein P, Cox P, Betts R et al. (2006) Climate–Carbon Cycle Feedback Analysis: Results from the C4MIP Model Intercomparison. *Journal of Climate,* **19**, 3337–3353.

Friend AD, Lucht W, Rademacher TT et al. (2014) Carbon residence time dominates uncertainty in terrestrial vegetation responses to future climate and atmospheric CO2. *Proceedings of the National Academy of Sciences,* **111**, 3280–3285.

de Goncalves LG de, Baker I, Christoffersen B et al. (2009) The Large Scale Biosphere-Atmosphere Experiment in Amazônia, Model Intercomparison Project (LBA-MIP) protocol.

de Gonçalves LGG, Borak JS, Costa MH et al. (2013) Overview of the Large-Scale Biosphere–Atmosphere Experiment in Amazonia Data Model Intercomparison Project (LBA-DMIP). *Agricultural and Forest Meteorology,* **182–183**, 111–127.

Gotangco Castillo CK, Levis S, Thornton P (2012) Evaluation of the New CNDV Option of the Community Land Model: Effects of Dynamic Vegetation and Interactive Nitrogen on CLM4 Means and Variability*. *Journal of Climate,* **25**, 3702–3714.

Gower ST, Kucharik CJ, Norman JM (1999) Direct and Indirect Estimation of Leaf Area Index, fAPAR, and Net Primary Production of Terrestrial Ecosystems. *Remote Sensing of Environment,* **70**, 29–51.

Guan K, Pan M, Li H et al. (2015) Photosynthetic seasonality of global tropical forests constrained by hydroclimate. *Nature Geoscience,* **8**, 284–289.

Hodnett MG, Oyama MD, Tomasella J, Marques A de OF (1996) Comparisons of long-term soil water storage behavior under pasture and forest in three areas of Amazonia. In: Amazonia

Deforestation and Climate. In: *Amazonian Deforestation and Climate*, eds Gash JHC edn, , Nobre CA edn, , Roberts JM edn, , Victoria RL edn, pp. 57–77. John Wiley, New York, USA.

Huete AR, Didan K, Shimabukuro YE et al. (2006) Amazon rainforests green-up with sunlight in dry season. *Geophysical Research Letters*, **33**, L06405.

Huffman GJ, Bolvin DT, Nelkin EJ et al. (2007) The TRMM Multisatellite Precipitation Analysis (TMPA): Quasi-Global, Multiyear, Combined-Sensor Precipitation Estimates at Fine Scales. *Journal of Hydrometeorology*, **8**, 38–55.

Huntingford C, Zelazowski P, Galbraith D et al. (2013) Simulated resilience of tropical rainforests to CO2-induced climate change. *Nature Geoscience*, **6**, 268–273.

Hutyra LR, Munger JW, Saleska SR et al. (2007) Seasonal controls on the exchange of carbon and water in an Amazonian rain forest. *Journal of Geophysical Research: Biogeosciences*, **112**, 1–16.

Ju W, Chen JM, Black TA, Barr AG, Liu J, Chen B (2006) Modelling multi-year coupled carbon and water fluxes in a boreal aspen forest. *Agricultural and Forest Meteorology*, **140**, 136–151.

Khomik M, Arain MA, Brodeur JJ, Peichl M, Restrepo-Coupé N, McLaren JD (2010) Relative contributions of soil, foliar, and woody tissue respiration to total ecosystem respiration in four pine forests of different ages. *Journal of Geophysical Research: Biogeosciences*, **115**, 1–17.

Kim Y, Knox RG, Longo M et al. (2012) Seasonal carbon dynamics and water fluxes in an Amazon rainforest. *Global Change Biology*, **18**, 1322–1334.

Kruijt B, Elbers JA, von Randow C et al. (2004) The Robustness of Eddy Correlation Fluxes for Amazon Rain Forest Conditions. *Ecological Applications*, **14**, 101–113.

Kucharik CJ, Barford CC, Maayar ME, Wofsy SC, Monson RK, Baldocchi DD (2006) A multiyear evaluation of a Dynamic Global Vegetation Model at three AmeriFlux forest sites: Vegetation structure, phenology, soil temperature, and CO_2 and H_2O vapor exchange. *Ecological Modelling,* **196**, 1–31.

Malhi Y, Pegoraro E, Nobre AD, Pereira MGP, Grace J, Culf AD, Clement R (2002) Energy and water dynamics of a central Amazonian rain forest. *Journal of Geophysical Research,* **107**, LBA 45-1–LBA 45-17.

Manabe S, Bryan K (1969) Climate Calculations with a Combined Ocean-Atmosphere Model. *Journal of the Atmospheric Sciences,* **26**, 786–789.

Medvigy D, Wofsy SC, Munger JW, Hollinger DY, Moorcroft PR (2009) Mechanistic scaling of ecosystem function and dynamics in space and time: Ecosystem Demography model version 2. *Journal of Geophysical Research: Biogeosciences,* **114**, G01002.

Melton JR, Shrestha RK, Arora VK (2015) The influence of soils on heterotrophic respiration exerts a strong control on net ecosystem productivity in seasonally dry Amazonian forests. *Biogeosciences,* **12**, 1151–1168.

Metcalfe DB, Meir P, Aragão LEOC et al. (2007) Factors controlling spatio-temporal variation in carbon dioxide efflux from surface litter, roots, and soil organic matter at four rain forest sites in the eastern Amazon. *Journal of Geophysical Research,* **112**, 1–9.

NASA (2014) Tropical Rainfall Measuring Mission Project (TRMM), 3B43: Monthly 0.25x0.25 degree merged TRMM and other estimates v7. *NASA Distrib. Active Arch. Cent., Goddard Space Flight Cent. Earth Sci., Greenbelt, Md.*

Niu D G-Y, Zeng DX (2012) Earth System Model, Modeling the Land Component of. In: *Climate Change Modeling Methodology* (ed Rasch PJ), pp. 139–168. Springer New York.

Oleson KW, Niu G-Y, Yang Z-L et al. (2008) Improvements to the Community Land Model and

their impact on the hydrological cycle. *Journal of Geophysical Research,* **113**, 1–26.

Parolin P (2000) Phenology and CO2-assimilation of trees in Central Amazonian floodplains. *Journal of Tropical Ecology,* **16**, 465–473.

Pitman AJ (2003) The evolution of, and revolution in, land surface schemes designed for climate models. *International Journal of Climatology,* **23**, 479–510.

Powell TL, Galbraith DR, Christoffersen BO et al. (2013) Confronting model predictions of carbon fluxes with measurements of Amazon forests subjected to experimental drought. *New Phytologist,* **200**, 350–365.

Rammig A, Jupp T, Thonicke K et al. (2010) Estimating the risk of Amazonian forest dieback. *New Phytologist,* **187**, 694–706.

von Randow C, Manzi AO, Kruijt B et al. (2004) Comparative measurements and seasonal variations in energy and carbon exchange over forest and pasture in South West Amazonia. *Theoretical and Applied Climatology,* **78**, 5–26.

von Randow C, Zeri M, Restrepo-Coupe N et al. (2013) Inter-annual variability of carbon and water fluxes in Amazonian forest, Cerrado and pasture sites, as simulated by terrestrial biosphere models. *Agricultural and Forest Meteorology,* **182–183**, 145–155.

Restrepo-Coupe N, da Rocha HR, da Araujo AC et al. (2013) What drives the seasonality of photosynthesis across the Amazon basin? A cross-site analysis of eddy flux tower measurements from the Brasil flux network. *Agricultural and Forest Meteorology,* **182-183**, 128–144.

Rice AH, Pyle EH, Saleska SR et al. (2004) Carbon balance and vegetation dynamics in an old-growth Amazonian forest. *Ecological Applications,* **14**, S55–S71.

Richardson AD, Carbone MS, Huggett BA et al. (2015) Distribution and mixing of old and new nonstructural carbon in two temperate trees. *The New Phytologist,* **206**, 590–597.

da Rocha HR, Goulden ML, Miller SD, Menton MC, Pinto LDVO, de Freitas HC, e Silva Figueira AM (2004) Seasonality of Water and Heat Fluxes over a Tropical Forest in Eastern Amazonia. *Ecological Applications*, **14**, 22–32.

da Rocha HR, Manzi AO, Cabral OM et al. (2009) Patterns of water and heat flux across a biome gradient from tropical forest to savanna in Brazil. *Journal of Geophysical Research: Biogeosciences*, **114**, G00B12.

Rowland L, Malhi Y, Silva-Espejo JE et al. (2013) The sensitivity of wood production to seasonal and interannual variations in climate in a lowland Amazonian rainforest. *Oecologia*, **174**, 295–306.

Sakaguchi K, Zeng X, Christoffersen BJ, Restrepo-Coupe N, Saleska SR, Brando PM (2011) Natural and drought scenarios in an east central Amazon forest: Fidelity of the Community Land Model 3.5 with three biogeochemical models. *Journal of Geophysical Research*, **116**, 1–24.

Saleska SR, Miller SD, Matross DM (2003) Carbon in Amazon forests: Unexpected seasonal fluxes and disturbance-induced losses. *Science*, **302**, 1554–1557.

Shao P, Zeng X, Sakaguchi K, Monson RK, Zeng X (2013) Terrestrial Carbon Cycle: Climate Relations in Eight CMIP5 Earth System Models. *Journal of Climate*, **26**, 8744–8764.

Shuttleworth WJ (1988) Evaporation from Amazonian Rainforest. *Proceedings of the Royal Society of London. Series B, Biological Sciences*, **233**, 321–346.

Sitch S, Smith B, Prentice IC et al. (2003) Evaluation of ecosystem dynamics, plant geography and terrestrial carbon cycling in the LPJ dynamic global vegetation model. *Global Change Biology*, **9**, 161–185.

Sobrado MA (1994) Leaf age effects on photosynthetic rate, transpiration rate and nitrogen content in a tropical dry forest. *Physiologia Plantarum*, **90**, 210–215.

Sombroek W (2001) Spatial and temporal patterns of Amazon rainfall. Consequences for the planning of agricultural occupation and the protection of primary forests. *Ambio*, **30**, 388–396.

Stoy PC, Katul GG, Siqueira MBS, Juang J-Y, Novick KA, Uebelherr JM, Oren R (2006) An evaluation of models for partitioning eddy covariance-measured net ecosystem exchange into photosynthesis and respiration. *Agricultural and Forest Meteorology*, **141**, 2–18.

Wagner F, Rossi V, Stahl C, Bonal D, Hérault B (2012) Water Availability Is the Main Climate Driver of Neotropical Tree Growth. *PLoS ONE*, **7**, e34074.

Wang W, Ciais P, Nemani RR et al. (2013) Variations in atmospheric CO2 growth rates coupled with tropical temperature. *Proceedings of the National Academy of Sciences of the United States of America*, **110**, 13061–13066.

Wang X, Piao S, Ciais P et al. (2014) A two-fold increase of carbon cycle sensitivity to tropical temperature variations. *Nature*, **506**, 212–215.

Werth D, Avissar R (2002) The local and global effects of Amazon deforestation. *Journal of Geophysical Research*, **107**, LBA 55–1–LBA 55–8.

Williams M, Richardson AD, Reichstein M et al. (2009) Improving land surface models with FLUXNET data. *Biogeosciences*, **6**, 1341–1359.

Wu J, Albert L, Lopes AP et al. (submitted) Leaf ontogeny and demography explain photosynthetic seasonality in Amazon evergreen forests. *Nature*.

Würth MKR, Peláez-Riedl S, Wright SJ, Körner C (2005) Non-structural carbohydrate pools in a tropical forest. *Oecologia*, **143**, 11–24.

668